ChemPubSoc Europe

DOI: 10.1002/chem.201600176

CHEMISTRY A European Journal Full Paper

Self-Assembly

Control over the Self-Assembly Modes of Pt^{II} Complexes by Alkyl Chain Variation: From Slipped to Parallel π-Stacks

Naveen Kumar Allampally,[a] María José Mayoral,[a, b] Sarayute Chansai,[c] María Cristina Lagunas,[c] Christopher Hardacre,[c] Vladimir Stepanenko,[a] Rodrigo Q. Albuquerque,[d] and Gustavo Fernández*[a, e]

Dedicated to Professor Nazario Martín on the occasion of his 60th birthday

Abstract: We report the self-assembly of a new family of hydrophobic, bis(pyridyl) Pt^{II} complexes featuring an extended oligophenyleneethynylene-derived π-surface appended with six long (dodecyloxy (**2**)) or short (methoxy (**3**)) side groups. Complex **2**, containing dodecyloxy chains, forms fibrous assemblies with a slipped arrangement of the monomer units ($d_{Pt\cdots Pt} \approx 14$ Å) in both nonpolar solvents and the solid state. Dispersion-corrected PM6 calculations suggest that this organization is driven by cooperative π–π, C–H···Cl and π–Pt interactions, which is supported by EXAFS and 2D NMR spectroscopic analysis. In contrast, nearly parallel π-stacks ($d_{Pt\cdots Pt} \approx 4.4$ Å) stabilized by multiple π–π and C–H···Cl contacts are obtained in the crystalline state for **3** lacking long side chains, as shown by X-ray analysis and PM6 calculations. Our results reveal not only the key role of alkyl chain length in controlling self-assembly modes but also show the relevance of Pt-bound chlorine ligands as new supramolecular synthons.

Introduction

Understanding the noncovalent forces that govern the formation of self-assembled structures and, in particular, supramolecular polymers,[1] is a prerequisite to construct functional materials, with optoelectronics and biomedicine being two of the most prosperous research fields in this regard.[2] To achieve these functionalities, highly ordered, adaptive nanostructures formed through a cooperative supramolecular polymerization mechanism are highly desirable.[3] The introduction of orthogonal noncovalent interactions,[4] from which hydrogen bonding and combinations with other secondary interactions are by far the most exploited,[5] represents a rational means for this purpose. The majority of these systems include purely organic building blocks, whereas the role of metal ions and polarized metal-bound atoms has been explored to a much lesser extent.

Square-planar Pt^{II} compounds are particularly relevant systems in this context because of their exceptional physicochemical, redox, catalytic, anticancer, and supramolecular properties.[6] These systems have a strong propensity to aggregate in both solution and in the solid state through Pt···Pt and/or other secondary forces, as recently shown for various classes of complexes in a comprehensive review by Yam and co-workers.[7] Among them, the self-assembly features of hydrophobic Pt^{II} complexes with acetylide,[8] bidentate,[9] tridentate N-donor,[10] and cyclometalating ligands[11] are relatively well understood.[7] In contrast, their hydrophobic counterparts featuring nonchelating ligands and, in particular, bis(pyridyl) Pt^{II} complexes have been limited to liquid crystalline materials[12] and hydrogen-bonded metallo-gelators.[13] Thus, there is a need for a deeper understanding of this class of Pt^{II} complexes, not only with respect to the nature of the metal ion but also regarding a wide range of weak unconventional forces stemming from the ligands attached to the metal fragment.[14] Such understanding may lead to the discovery of new supramolecular synthons.

[a] Dr. N. K. Allampally, Dr. M. J. Mayoral, Dr. V. Stepanenko, Prof. Dr. G. Fernández
Institut für Organische Chemie and
Center for Nanosystems Chemistry, Universität Würzburg
Am Hubland, 97074 Würzburg (Germany)

[b] Dr. M. J. Mayoral
Current address: Departamento de Química Orgánica
Facultad de Ciencias, Universidad Autónoma de Madrid
28049 Madrid (Spain)

[c] Dr. S. Chansai, Dr. M. C. Lagunas, Prof. C. Hardacre
School of Chemistry and Chemical Engineering
Queen's Universtity Belfast, Stranmillis Road
Belfast BT9 5AG (United Kingdom)

[d] Prof. R. Q. Albuquerque
São Carlos Institute of Chemistry, University of São Paulo
Av. Trab. São-Carlense, 400, 13560-970 São Carlos-SP (Brazil)

[e] Prof. Dr. G. Fernández
Current address: Organisch-Chemisches Institut
Westfälische Wilhelms-Universität Münster
Corrensstrasse 40, 48149 Münster (Germany)
E-mail: fernandg@uni-muenster.de

Supporting information for this article can be found under http://dx.doi.org/10.1002/chem.201600176. It includes synthesis and characterization, additional UV Vis studies, cooling curves, 1D and 2D NMR spectra, PM6 calculations, gelation studies, SEM, AFM, WAXS, X-ray diffraction and EXAFS.

In this article, we report a new family of hydrophobic bis(pyridyl)dichloride Pt^{II} complexes exhibiting a large aromatic oligophenyleneethynylene (OPE)-based platform and peripheral dodecyloxy (**2**) and methoxy (**3**) chains. The remarkably different molecular arrangement of **2** and **3** underlines the conclusion that alkyl chain length plays an important role in the self-assembly,[15] as also previously observed for Pt^{II} complexes with tridentate ligands.[16] This has been demonstrated by applying a battery of experimental methods, including temperature-dependent UV/Vis and ^{1}H NMR spectroscopy, ROESY NMR spectroscopy, atomic force microscopy (AFM), scanning electron microscopy (SEM), wide angle X-ray scattering (WAXS), extended X-ray absorption fine structure (EXAFS), X-ray diffraction, and dispersion-corrected PM6 quantum chemical calculations.

In nonpolar solvents, slipped π-stacks driven by cooperative π–π, C–H···Cl, and π–Pt contacts are formed for **2**, whereas nearly parallel stacks with Pt···Pt distances of 4.4 Å are obtained in the crystal structure of **3**. In contrast to our previously reported, structurally related bis(pyridyl)dichloride Pd^{II} complexes,[17] these studies demonstrate that not only the presence or absence of peripheral chains but also the nature of the metal ion (Pt^{II}) is responsible for the rearrangement of the molecules into various packing modes.

Results and Discussion

OPE-based pyridyl ligand **1a** featuring dodecyloxy chains was previously synthesized according to reported procedures,[17] whereas its homologue with shorter methoxy groups (**1b**) was obtained by a sequence of cross-coupling reactions and selective deprotection protocols (see the Supporting Information). The target OPE-based Pt^{II} complexes **2**–**3** were successfully obtained in very good yields by heating a mixture of **1a**–**b** (2 equiv) and $Pt(PhCN)_2Cl_2$ (1 equiv) to reflux in anhydrous benzene for 2–3 days under N_2 gas (Scheme 1). Complexes **2** and **3** have been well characterized by NMR and IR spectroscopy, HRMS, elemental analyses, and X-ray diffraction analysis (for **3**) (see further details in the Supporting Information). Both complexes are nonemissive in solution, in line with our previous reports.[17]

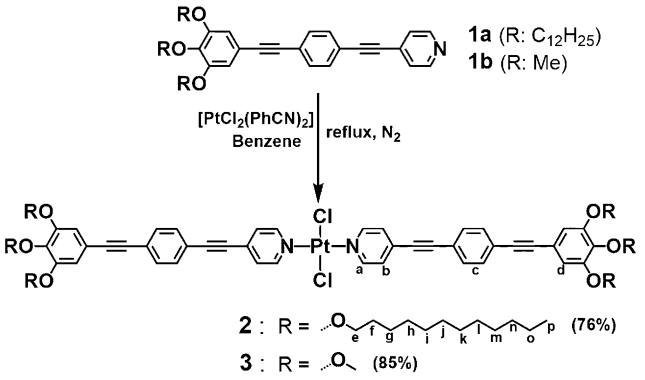

Scheme 1. Synthetic route to obtain Pt^{II} complexes **2** and **3**.

UV/Vis measurements of **2** were recorded in solvents of different polarity (tetrahydrofuran (THF), $CHCl_3$, dichloromethane (CH_2Cl_2), cyclohexane (CHY) and methylcyclohexane (MCH)) to observe the solvent dependency of the spectra (Figure 1a and S1). In all solvents at a concentration of approximately 9×10^{-6} M, complex **2** shows two transitions with maxima at 285 and 360 nm. The former can be assigned to a typical ligand-centered transition (^{1}LC, π–π*, 275–315 nm), whereas the latter is due to metal to ligand charge transfer (^{1}MLCT, 320–380 nm).[18] Intriguingly, there is no particular effect of the polarity of the solvent on the absorption maxima at this concentration in the investigated solvents. An increase in concentration to 1×10^{-4} M does not lead to significant spectral changes, with the exception of MCH, in which noticeable spectral changes in the course of temperature-dependent experiments at a concentration of 5×10^{-5} M were observed. The position of the maximum redshifts from 360 to 377 nm, while a new sharp transition rises around 410 nm on reducing the temperature from 340 to 273 K (Figure 1a and S1–S2). This particular phenomenon suggests that aggregation does occur and we have observed that it is thermally reversible. Thus, **2** still exists in the monomeric state in THF, $CHCl_3$, and CH_2Cl_2 even at higher concentrations (good solvents), whereas self-assembled species form in MCH (hydrophobic solvent). To confirm that the redshifted band at 377 nm and the sharp shoulder at ca. 410 nm

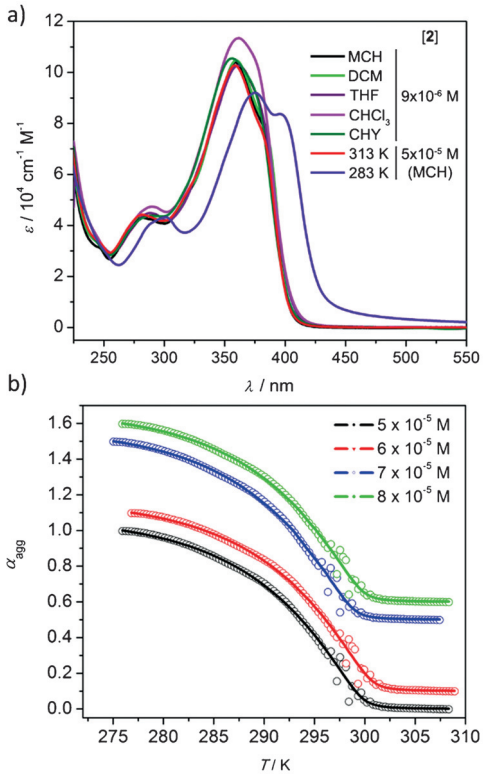

Figure 1. a) Absorption spectra of **2** in various solvents (9×10^{-6} M) at room temperature and in MCH (conc. 5×10^{-5} M) at two temperatures (313 K (red) and 283 K (purple)). b) Cooling curves at different concentrations of **2** in MCH, fitting of α_{agg} vs. T in the framework of the ten Eikelder–Markvoort–Meijer model. The red, blue, and green curves have been vertically shifted slightly for better visualization.

are due to aggregation, thin films were prepared from CH_2Cl_2 and MCH. The UV/Vis spectrum of a thin film from CH_2Cl_2 showed the representative spectral features of a molecularly dissolved state; that is, an absorption maximum at ca. 360 nm (Figure S1). The position of this maximum matches well with that observed in MCH at high temperatures. In sharp contrast and similar to the behavior in MCH solution at low temperatures, the thin film from MCH presents a redshifted aggregate band at 377 nm along with a new shoulder at 400 nm, confirming the formation of self-assembled species in this medium (Figure S1).

To closely follow the self-assembly process in MCH solution, we have monitored the spectral changes at a given wavelength (400 nm) by slowly cooling MCH solutions (conc. 5–8 $\times 10^{-5}$ M) of **2** from 323 to 274 K. To verify that the self-assembly progresses under thermodynamic control, a cooling rate of 1 K min^{-1} was chosen. A particularly interesting temperature range of the self-assembly process was 315–276 K, at which a clear transition from monomeric to aggregated species was observed, yielding nonsigmoidal cooling curves (see Figure 1 b).

To calculate the thermodynamic parameters, the obtained cooling curves were fitted to the ten Eikelder–Markvoort–Meijer model:[19] the results confirmed that the self-assembly mechanism of **2** is a highly cooperative phenomenon (Figure 1 b and S2). The corresponding thermodynamic parameters are displayed in Table 1. This model assumes that nuclei of two molecules of **2** are formed in the first unfavorable nucleation step, which is followed by a much more favorable elongation into supramolecular polymeric nanostructures. According to the thermodynamic analysis, the dimerization constants (K_d) range from 4.7 to 20.2 M^{-1}, whereas the elongation constants (K_e) are around 1000-fold higher (1.77–2.25 $\times 10^4$ M). The quotient between the nucleation and elongation constants yields low values of σ (2.6–8.9 $\times 10^{-4}$), which denote a high degree of cooperativity (for a global analysis of the fits see Table 1, bottom). By comparing these thermodynamic parameters with those calculated for a structurally related OPE-based bis(pyridyl)dichloride Pd^{II} investigated by our group,[17] slight differences can be noted. For instance, the K_d for Pt^{II} complex **2** is approximately two orders of magnitude higher (ca. 0.65 vs. ca. 100 M^{-1}), whereas the K_e is around three times higher (ca. 7.7 $\times 10^3$ vs. ca. 2 $\times 10^4$ M^{-1}) than those obtained for the analogous Pd^{II} derivative. This demonstrates that the nature of the metal ion plays a role in the self-assembly and degree of cooperativity.

Given that the self-assembly process is observed to be cooperative, the aggregate growth should be governed by the interplay of various orthogonal noncovalent interactions.[4] The presence of an extended aromatic surface in **2** indicates that strong π–π interactions will be a major contribution to the supramolecular polymerization. According to literature precedent, we hypothesized that either metal···metal[17] or weak interactions[14b] involving the Cl-Pt^{II}-Cl fragment of **2** could represent additional forces to the cooperative growth. To investigate this further, temperature-dependent ^{1}H NMR and 2D-NMR spectroscopic measurements were performed in [D_{14}]MCH. Variable-temperature ^{1}H NMR studies (8 mM, 400 MHz, 351–308 K) show a slight upfield shift of most aromatic signals with decreasing temperature, in particular those corresponding to the H_a protons of the pyridine rings, suggesting that π-stacking interactions are involved in the self-assembly process (Figure S3).

By comparing the COSY and ROESY spectra (Figure S3–S4), we found new cross-peaks in the latter experiments that can be assigned to the coupling of some of the protons of the phenylene rings in the aggregate structure. Interestingly, protons H_d of the outer ring couple with protons H_a and H_b of the pyridine units (Figure 2 a), which is also predicted by theoretical calculations (see below). The appearance of these signals confirms that the units of **2** cannot be arranged into parallel stacks through π–π and Pt···Pt interactions, because the intermolecular distance between protons H_a and H_d (ca. 13 Å) would be much larger than the estimated distance ($\leq$ 5 Å) for nuclear spins to correlate. The results extracted from both 1D and 2D NMR experiments for **2** closely resemble those obtained for analogous amphiphilic Pt^{II} complexes investigated in our group.[14b] For these systems, the presence of polar glycol side chains induces a translational displacement of the OPE scaffolds within the supramolecular fiber driven by CH···O and CH···Cl weak hydrogen bonding involving the oxygen and hydrogen atoms of the polar chains. Thus, in the light of these results, it appears that the hydrophobic Pt^{II} complex **2** self-assembles in a similar fashion into slipped π-stacks in MCH solution, despite the absence of multiple polarizable oxygen atoms in the side chains. As a result, other secondary forces apart from π–π interactions should be necessarily involved to stabilize the stack, most likely interactions involving the Cl-Pt^{II}-Cl fragments and the aromatic rings of adjacent molecules.

Table 1. Thermodynamic parameters associated with the self-assembly of **2** at different concentrations.

Conc. [M]	ΔH°_{nucl} [kJ mol^{-1}]	ΔH° [kJ mol^{-1}]	ΔS° [kJ mol^{-1} K^{-1}]	T_e [K]	K_2 [M^{-1}]	K [M^{-1}]	σ
5×10^{-4}	-17.4 ± 0.3	-81.4 ± 0.5	-0.1898 ± 0.0017	299.1 ± 0.05	20.2	2.25×10^4	8.9×10^{-4}
6×10^{-4}	-17.5 ± 0.2	-90.5 ± 0.2	-0.2215 ± 0.0007	299.4 ± 0.03	16.9	1.97×10^4	8.6×10^{-4}
7×10^{-4}	-19.3 ± 0.1	-92.9 ± 0.2	-0.2303 ± 0.0006	300.0 ± 0.02	7.5	1.81×10^4	4.2×10^{-4}
8×10^{-4}	-20.4 ± 0.1	-100.2 ± 0.2	-0.2550 ± 0.0005	300.6 ± 0.02	4.7	1.77×10^4	2.6×10^{-4}
Global fitting[a]	-12.5 ± 0.5	-117.4 ± 2.7	-0.3130 ± 0.0091	298.4[c]	103.9	1.57×10^4	6.6×10^{-3}
Global fitting[b]	-12.2 ± 0.5	-119.7 ± 2.7	-0.3207 ± 0.0091	298.4[c]	113.4	1.55×10^4	7.3×10^{-3}

[a] Normalize data with single normalization constant. [b] Normalize each curve individually. [c] Average value.

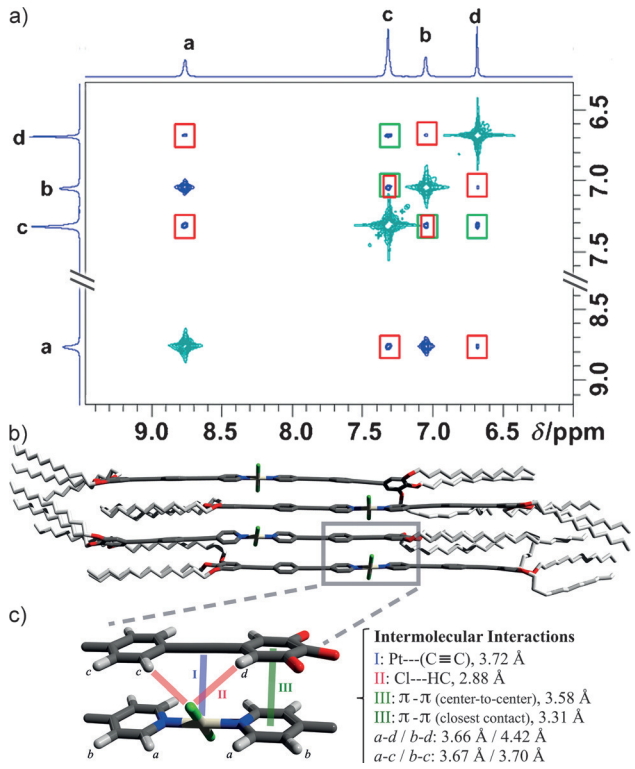

Figure 2. a) Partial ROESY NMR spectrum ([D_{14}]MCH, 600 MHz, 8.73 mM, 305 K) of **2**. The green and red squares highlight intra- and intermolecular through-space coupling signals, respectively. b) PM6 geometry-optimized structure of a tetramer of **2**. c) Enlarged section of the structure depicted in (b) showing the most relevant noncovalent interactions.

To analyze the possible noncovalent interactions that help maintain the slipped packing of **2** deduced by 2D NMR studies, quantum chemical calculations were performed at the PM6 semiempirical level with dispersion corrections[20] using the MOPAC program.[21] The optimized geometry of a tetramer of **2** is shown in Figure 2b, in which hydrogen atoms were omitted for clarity. It is clear how intermolecular van der Waals interactions among alkyl chains contribute to stabilize the stack. Aromatic interactions are also important here: four out of six aromatic rings of each monomer participate in such contacts. Intermolecular interactions between outer aromatic rings and alkyl chains (CH···π) are also observed in Figure 2b, for which many pairs of alkyl protons–H_a (see Scheme 1 for proton labeling) have distances of less than 5 Å. This is consistent with the correlation between most protons of the alkyl chains (H_{e-g}) and aromatic protons H_{a-d} obtained in the ROESY spectra (Figure S3). The intramolecular (H_c···H_d and H_b···H_c) and intermolecular (H_a···H_c and H_b···H_c) distances obtained from the optimized tetramer are also less than 5 Å, which agrees well with the ROESY signals found (Figure 2a). Heats of formation predicted from the PM6 calculations for aggregates of **2** with different numbers (n) of monomer units ($n = 1$–4) were used to estimate the following ΔH values (in kJ mol^{-1}) of monomer addition: −255 (1 + 1→2), −352 (2 + 1→3), and −377 (3 + 1→4) (Figure S5). These values suggest that subsequent monomer additions become increasingly more stable for longer aggregates, which is in line with the cooperativity observed experimentally.

Figure 2c shows an expanded region of the optimized tetramer, revealing different kinds of intermolecular interactions involving Cl, Pt, H–C, and aromatic moieties. Protons H_{a-d} are also labeled to show their close relative proximity, which explains why their 2D NMR signals are coupled (Figure 2a). The semiempirical calculations suggest that the slipped stacking depicted in Figure 2b is promptly destabilized if the alkyl chains are removed; that is, if **3** is used instead of **2** to build the same stack. The optimized geometry of an octamer of **3** built in the slipped arrangement evidences that outer aromatic rings of the first and third (or second and fourth, etc.) monomers in the stack would be strongly distorted to interact with each other (Figure S6). This distortion hampers further growth of the aggregate in the slipped arrangement, which nicely points out that the alkyl chains play a key role in the final arrangement of the supramolecular aggregate: the long side groups of **2** favor the slipped arrangement whereas the much shorter side groups of **3** appear to destabilize it (see below).

The hydrophobic character of **2** along with the existence of cooperative non-covalent forces are responsible for an effective and reversible gelation process in hydrophobic solvents such as hexane, isooctane, dodecane, and MCH. The sol–gel transitions in isooctane and dodecane gels are very spontaneous and instantaneous, whereas for the hexane and MCH gels, the recovery of the gel state from the sol requires at least 20 min standing at room temperature. Their respective critical gelation concentrations (CGC) were observed to decrease upon increasing the chain length of the solvent (see the Supporting Information), confirming that the gelation capacity of solvents containing shorter hydrocarbon chains is less effective.[22] The surface morphology of the gels has been investigated by means of SEM and AFM. The respective SEM and AFM images of xerogels displayed in Figure 3 and S7 confirm

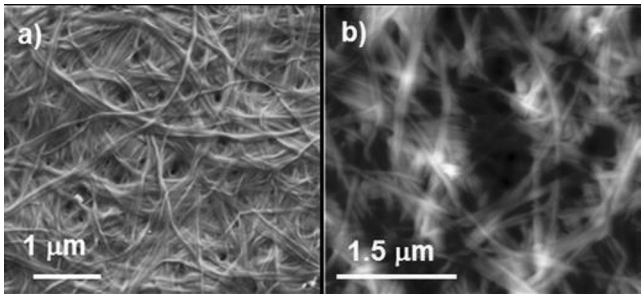

Figure 3. Surface morphology of xerogels of **2**. a) SEM image from a gel in isooctane. b) AFM of a dodecane gel on silicon wafer.

that the surface morphology is not significantly affected by the solvent. The length of the fibers is in the order of micrometers and the width ranges from 50 to 100 nm. WAXS studies of a gel of **2** in hexane display a reflection at $2\theta = 26.8^\circ$ that corresponds to a π–π distance of 3.3 Å between the units of **2** (Figure S8), in agreement with the values predicted by PM6 calculations.

To rationalize the influence of the alkyl side groups on the self-assembly of **2**, we have investigated the analogous Pt^{II}

complex **3**, lacking the dodecyloxy chains, by X-ray diffraction analysis. The removal of these chains facilitates substantially the realization of single crystals, in contrast to **2**, in which the presence of six long side groups cause a significant disorder in the crystal lattice. Unfortunately, the poor solubility of **3** in highly nonpolar solvents such as MCH and cyclohexane comes along with negligible gelation abilities and precludes a detailed analysis of the supramolecular polymerization mechanism (Figure S7a). For instance, cooling curves of **3** in MCH cannot be recorded even under dilute conditions (1×10^{-6} M) because the complex rapidly precipitates, thus precluding a suitable comparison with **2**. Suitable crystals of **3** for X-ray analysis were obtained by slow evaporation from a concentrated solution (ca. 1 mM) of CH_3CN and CH_2Cl_2 (1:1). Figure 4 shows the molecular arrangement of **3** in the crystal structure in four different views. Within the monomeric units of **3**, the OPE-based ligands are nearly coplanar, whereas the chlorine atoms attached to the Pt^{II} ion are slightly bent out of the plane to facilitate interactions with neighboring units of **3** (Figure 4a). This slightly distorted square-planar coordination is stabilized by two intramolecular C–H···Cl interactions (2.919 and 2.869 Å) between the H_a of the pyridine rings and the chlorine atoms of the same molecule (Figure S9). The packing of **3** in the crystal structure is primarily driven by intermolecular C–H(aromatic)···Cl and translationally stacked π–π interactions, because the relatively bulky chlorine atoms hinder the alignment of the units of **3** in a perfect parallel fashion through Pt···Pt bonding. Each chlorine atom is involved in three intermolecular (py)CH···Cl interactions with two neighboring monomers belonging to a parallel 1D stack ($d=3.09$ and 2.79 Å) and to one monomer inside the same stack ($d=2.76$ Å, Figure S9).

The three CH···Cl intermolecular contacts together with multiple π–π interactions (3.3 Å) involving the aromatic OPE rings facilitate the growth of the structure into 1D stacks (Figure 4a) and are responsible for the packing of the molecules as shown in Figure 4b–d. The molecular arrangement of **3** extracted from X-ray studies (Figure 4) is remarkably different when compared with that of **2** in MCH solution suggested by 2D NMR studies and theoretical calculations (Figure 2c), although for both systems the chlorine ligands are very important to stabilize the aggregates. Whereas **2** forms slipped stacks with $d_{Pt\cdots Pt} \approx 14$ Å, the removal of the long chains in **3** enables a tighter molecular arrangement into almost parallel stacks with much shorter distances between the Pt centers (4.4 Å). It is important to note that the Pt···(C≡C) interaction is exclusively found in aggregates of **2** and it can involve σ- and π-electron donations to Pt, as well as δ and π back-donations. This interaction can contribute to a certain extent to the stabilization of the slipped configuration found for **2**, even though the Pt···(C≡C) bond distances predicted by PM6 calculations are larger than those usually found in Pt^{II}-alkyne complexes. Although the molecular packing within a self-assembled structure and in the crystal state sometimes differ, our results evidence that the presence of flexible alkyl chains in **2** represents a major contribution to shifting the packing in solution, as already pointed out by the theoretical calculations.

Pt L_{III} extended EXAFS studies have been performed to further support the supramolecular assembly of **2** and to establish a correlation between the solid-state packing and solution/gel of **2** in both hexane and MCH. The k^3-weighted EXAFS spectra and Fourier transforms (FTs) for the three samples are shown in Figure S10. The theoretical models for the EXAFS were constructed by using crystallographic data from complex **3**, as well as from an analogous compound with unsubstituted pyridine ligands $[PtCl_2(py)_2]$.[23] The latter was chosen to reproduce the slipped molecular arrangement proposed for complex **2** (see Figure 2), in contrast to the almost parallel stacks with relatively short Pt···Pt distances (4.4 Å) observed in **3**. In particular, in the crystal packing of $[PtCl_2(py)_2]$, the molecules are organized in a such a way that two of the pyridine C atoms of one molecule are close to the Pt center of the adjacent molecule (ca. 3.6 Å, see Figure S10). Details of EXAFS data

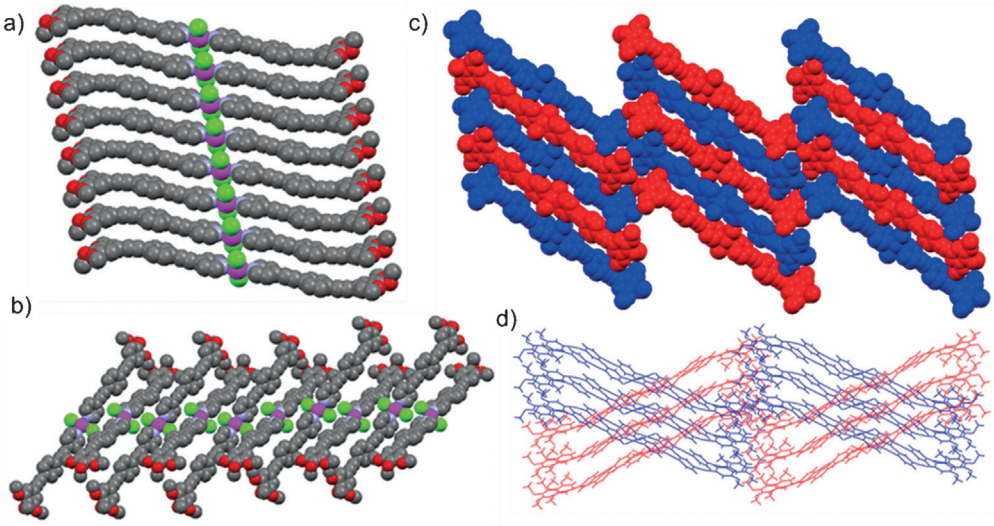

Figure 4. Arrangement of **3** in the crystal structure, a) vertical and b) horizontal views and c) 2D and d) 3D-packing. The hydrogen atoms have been omitted for clarity. Color codes: Pt: pink; Cl: green; O: red; N: light blue; C. gray.

analysis and of the scattering paths included in the theoretical models are provided in the Supporting Information (Tables S2–S5; Figure S11–S13).

Data and best-fit model for the EXAFS spectrum and FT for complex **2** in the solid state are shown in Figure 5. Structural information extracted from the EXAFS fittings is included in Table S3. The two main features in the FT at ca. 1.6 and 2 Å (Figure 5) correspond to single scatterings from the N and Cl atoms, respectively, whereas the next peaks at 2.3–2.8 Å correspond mainly to contributions of the pyridine *ortho*-C atoms (single and multiple scattering paths). The smaller features between 2.8 and 3.5 Å can be best fitted by including multiple scattering paths Pt→N→Cl and Pt→N→N.

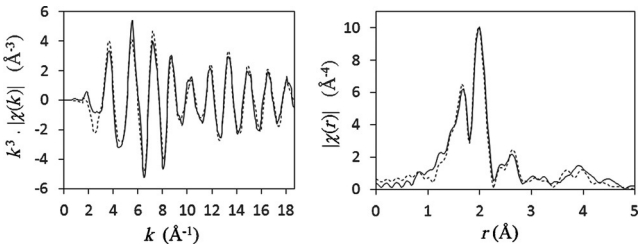

Figure 5. Data (solid line) and best-fit model (dotted line) for complex **2** in the solid state: k^3-Weighted EXAFS spectra (left) and magnitude of Fourier transform (right).

At this stage, the effect on the fitting of including contributions from other scattering paths from complex **3** and/or $[PtCl_2(py)_2]$ was carefully considered. The best fit was obtained by including additional scattering paths only from $[PtCl_2(py)_2]$, in particular single and multiple scatterings involving the C atoms at 3.6 Å of adjacent molecules (adj-C) and the pyridine *meta*-C atoms. These paths contributed to the FT of the data in the region between 3.5–4.5 Å. Inclusion of additional or alternative scattering paths did not make a significant difference in the fitting. Particularly, if Pt→Pt and Pt→*meta*-C single scattering paths from complex **3** are considered instead of the C contributions from $[PtCl_2(py)_2]$, the fit worsens. These results support the molecular aggregation deduced by 2D NMR spectroscopic analysis and quantum chemical calculations for complex **2** in solution, as discussed above. It should be noted that the Pt-adj-C distance determined by EXAFS for complex **2** (3.95 ± 0.02 Å) is longer than that in the crystal structure of $[PtCl_2(py)_2]$ (3.6 Å), and can be related to the bulky pyridine substituents in **2**. The EXAFS data for the gels in both hexane and MCH were then fitted by applying the same parameters used in the best-fit model for the solid sample. The results obtained were analogous to those of the solid, with the best fit achieved when using scattering from Pt→adjC, thus suggesting that the molecules in both gels aggregate in the same way as in the solid sample (Figure S12–S13, Tables S4–S5).

Conclusion

The self-assembly of a new family of hydrophobic π-conjugated (bis)pyridyl Pt^{II} complexes equipped with long (dodecyloxy, **2**) or short (methoxy, **3**) side groups is described. The collection of experimental and theoretical results show remarkable differences in the self-assembly modes depending on the alkyl group length. Whereas Pt^{II} complex **2** with long chains self-assembles into slipped π-stacks, the removal of the side groups in **3** enables a nearly parallel molecular arrangement with Pt···Pt distances of 4.4 Å. NMR studies, X-ray spectroscopic analysis, EXAFS, and PM6 calculations have given insight on the multiple intermolecular interactions (π–π, Cl···H, Pt···π) involved in both arrangements. For both complexes, the Cl atoms have been found to be fundamental to explain the driving force behind the self-assembly of **2** and **3**. Our findings show: 1) the key role of alkyl groups in controlling self-assembly modes, and 2) the establishment of metal-bound Cl atoms as a new synthon in the field of supramolecular chemistry. Our current efforts are focused on the preparation of a series of related Pt^{II} and Pd^{II} complexes with alkyl chains of variable length (between C_2H_5 and $C_{18}H_{37}$) to establish the critical chain length responsible for the self-assembly switch.

Acknowledgements

We thank the Humboldt Foundation (Sofja Kovalevskaja Award) and the Brazilian agencies CAPES (A061_2013) and CNPq (305082/2013-2) for financial support. We thank Professor Frank Würthner for helpful discussions and Dr. David Schmidt for crystal structure analysis. We gratefully acknowledge Diamond Light Source (Oxfordshire, U.K.) (Experiment number (EXP 9223), beamline (BL AP14)).

Keywords: cooperative effects · noncovalent interactions · pi-interactions · self-assembly · solid-state structures

[1] a) L. Yang, X. Tan, Z. Wang, X. Zhang, *Chem. Rev.* **2015**, *115*, 7196 – 7239; b) P. Wei, X. Yan, F. Huang, *Chem. Soc. Rev.* **2015**, *44*, 815 – 832; c) C. Kulkarni, S. Balasubramanian, S. J. George, *ChemPhysChem* **2013**, *14*, 661 – 673; d) T. F. A. De Greef, M. M. J. Smulders, M. Wolffs, A. P. H. J. Schenning, R. P. Sijbesma, E. W. Meijer, *Chem. Rev.* **2009**, *109*, 5687 – 5754.

[2] a) F. Würthner, C. R. Saha-Möller, B. Fimmel, S. Ogi, P. Leowanawat, D. Schmidt, *Chem. Rev.* **2015**, *116*, 962 – 1052; b) S. Yagai, *Bull. Chem. Soc. Jpn.* **2015**, *88*, 28 – 58; c) J. Schill, A. P. H. J. Schenning, L. Brunsveld, *Macromol. Rapid Commun.* **2015**, *36*, 1306 – 1321; d) A. S. Tayi, A. Kaeser, M. Matsumoto, T. Aida, S. I. Stupp, *Nat. Chem.* **2015**, *7*, 281 – 294; e) K. Müllen, *ACS Nano* **2014**, *8*, 6531 – 6541; f) S. S. Babu, V. K. Praveen, A. Ajayaghosh, *Chem. Rev.* **2014**, *114*, 1973 – 2129; g) W. Li, Y. Kim, J. Li, M. Lee, *Soft Matter* **2014**, *10*, 5231 – 5242; h) M. R. Molla, S. Ghosh, *Phys. Chem. Chem. Phys.* **2014**, *16*, 26672 – 26683; i) A. Das, S. Ghosh, *Angew. Chem. Int. Ed.* **2014**, *53*, 2038 – 2054; *Angew. Chem.* **2014**, *126*, 2068 – 2084; j) J. Boekhoven, S. I. Stupp, *Adv. Mater.* **2014**, *26*, 1642 – 1659; k) P. A. Korevaar, T. F. A. De Greef, E. W. Meijer, *Chem. Mater.* **2014**, *26*, 576 – 586; l) B. Rybtchinski, *Adv. Polym. Sci.* **2013**, *262*, 363 – 387; m) E. Busseron, Y. Ruff, E. Moulin, N. Giuseppone, *Nanoscale* **2013**, *5*, 7098 – 7140.

[3] T. Aida, E. W. Meijer, S. I. Stupp, *Science* **2012**, *335*, 813 – 817.

[4] C. Rest, R. Kandanelli, G. Fernández, *Chem. Soc. Rev.* **2015**, *44*, 2543 – 2572.

[5] D. Gonzalez-Rodriguez, A. P. H. J. Schenning, *Chem. Mater.* **2011**, *23*, 310 – 325.

[6] a) C.-N. Lok, T. Zou, J.-J. Zhang, I. W.-S. Lin, C.-M. Che, *Adv. Mater.* **2014**, *26*, 5550 – 5557; b) M. Mauro, A. Aliprandi, D. Septiadi, N. S. Kehra, L. De Cola, *Chem. Soc. Rev.* **2014**, *43*, 4144 – 4166; c) W. Wang, H.-B. Yang, *Chem. Commun.* **2014**, *50*, 5171 – 5186; d) N. Lanigan, X. S. Wang, *Chem.*

Commun. **2013**, *49*, 8133 – 8144; e) A. Y.-Y. Tam, V. W.-W. Yam, *Chem. Soc. Rev.* **2013**, *42*, 1540 – 1567; f) K. M.-C. Wong, V. W.-W. Yam, *Acc. Chem. Res.* **2011**, *44*, 424 – 434; g) I. Eryazici, C. N. Moorefield, G. R. Newkome, *Chem. Rev.* **2008**, *108*, 1834 – 1895; h) J. A. G. Williams, *Top. Curr. Chem.* **2007**, *281*, 205 – 268; i) S. W. Lai, C. M. Che, *Top. Curr. Chem.* **2004**, *241*, 27 – 63; j) N. Kimizuka, *Adv. Mater.* **2000**, *12*, 1461 – 1463.

[7] V. W.-W. Yam, V. K.-M. Au, S. Y.-L. Leung, *Chem. Rev.* **2015**, *115*, 7589 – 7728.

[8] a) N. K. Allampally, C.-G. Daniliuc, C. A. Strassert, L. De Cola, *Inorg. Chem.* **2015**, *54*, 1588 – 1596; b) Y.-K. Tian, Y.-G. Shi, Z.-S. Yang, F. Wang, *Angew. Chem. Int. Ed.* **2014**, *53*, 6090 – 6094; *Angew. Chem.* **2014**, *126*, 6204 – 6208; c) M. Mauro, A. Aliprandi, C. Cebrián, D. Wang, C. Kübel, L. De Cola, *Chem. Commun.* **2014**, *50*, 7269 – 7272; d) H.-L. Au-Yeung, S. Y.-L. Leung, A. Y.-Y. Tam, V. W.-W. Yam, *J. Am. Chem. Soc.* **2014**, *136*, 17910 – 17913; e) S. Y.-L. Leung, W. H. Lam, V. W.-W. Yam, *Proc. Natl. Acad. Sci. USA* **2013**, *110*, 7986 – 7991.

[9] a) C.-F. Ng, H.-F. A. Chow, *Chem. Commun.* **2015**, *51*, 2349 – 2352; b) Y.-J. Tian, E. W. Meijer, F. Wang, *Chem. Commun.* **2013**, *49*, 9197 – 9199; c) X.-D. Xu, J. Zhang, L.-J. Chen, X.-L. Zhao, D.-X. Wang, H.-B. Yang, *Chem. Eur. J.* **2012**, *18*, 1659 – 1667.

[10] a) M. Krikorian, S. Liu, T. M. Swager, *J. Am. Chem. Soc.* **2014**, *136*, 2952 – 2955; b) I. Stengel, C. A. Strassert, L. De Cola, P. Bäuerle, *Organometallics* **2014**, *33*, 1345 – 1355; c) K.-C. Chang, J.-L. Lin, Y.-T. Shen, C.-Y. Hung, C.-Y. Chen, S.-S. Sun, *Chem. Eur. J.* **2012**, *18*, 1312 – 1321.

[11] a) S. Y.-L. Leung, E. S.-H. Lam, W. H. Lam, K. M.-C. Wong, W.-T. Wong, V. W.-W. Yam, *Chem. Eur. J.* **2013**, *19*, 10360 – 10369; b) A. K.-W. Chan, E. S.-H. Lam, A. Y.-Y. Tam, D. P.-K. Tsang, W. H. Lam, M.-Y. Chan, W.-T. Wong, V. W.-W. Yam, *Chem. Eur. J.* **2013**, *19*, 13910 – 13924; c) S. C.-F. Kui, F. F. Hung, S. L. Lai, M. Y. Yuen, C. C. Kwok, K. H. Low, S. S. Y. Chui, C.-M. Che, *Chem. Eur. J.* **2012**, *18*, 96 – 109.

[12] a) L. Plasseraud, L. C. Gonzalez, D. Guillon, G. Süss-Fink, R. Deschenaux, D. W. Bruce, B. Donnio, *J. Mater. Chem.* **2002**, *12*, 2653 – 2658; b) C. Mongin, B. Donnio, D. W. Bruce, *J. Am. Chem. Soc.* **2001**, *123*, 8426 – 8427; c) B. Donnio, D. W. Bruce, *J. Chem. Soc. Dalton Trans.* **1997**, 2745 – 2755.

[13] a) M. Chen, C. Wei, X. Wu, M. Khan, N. Huang, G. Zhang, L. Li, *Chem. Eur. J.* **2015**, *21*, 4213 – 4217; b) M. Chen, C. Wei, J. Tao, X. Wu, N. Huang, G. Zhang, L. Li, *Chem. Eur. J.* **2014**, *20*, 2812 – 2818.

[14] a) V. Stepanenko, R. Kandanelli, S. Uemura, F. Würthner, G. Fernández, *Chem. Sci.* **2015**, *6*, 5853 – 5858; b) C. Rest, M. J. Mayoral, K. Fucke, J. Schellheimer, V. Stepanenko, G. Fernández, *Angew. Chem. Int. Ed.* **2014**, *53*, 700 – 705; *Angew. Chem.* **2014**, *126*, 716 – 722.

[15] For an interesting report of side chain effects on crystal packing, see: A. D. Finke, D. E. Gross, A. Han, J. S. Moore, *J. Am. Chem. Soc.* **2011**, *133*, 14063 – 14070.

[16] a) C. Po, A. Y.-Y. Tam, V. W.-W. Yam, *Chem. Sci.* **2014**, *5*, 2688 – 2695; b) C. Po, A. Y.-Y. Tam, K. M.-C. Wong, V. W.-W. Yam, *J. Am. Chem. Soc.* **2011**, *133*, 12136 – 12143.

[17] M. J. Mayoral, C. Rest, V. Stepanenko, J. Schellheimer, R. Q. Albuquerque, G. Fernández, *J. Am. Chem. Soc.* **2013**, *135*, 2148 – 2151.

[18] Y. Zhao, G. Roberts, S. Greenough, N. Farrer, M. Paterson, W. Powell, V. Stavros, P. Sadler, *Angew. Chem. Int. Ed.* **2012**, *51*, 11263 – 11266; *Angew. Chem.* **2012**, *124*, 11425 – 11428.

[19] a) A. J. Markvoort, H. M. M. ten Eikelder, P. A. Hilbers, T. F. A. de Greef, E. W. Meijer, *Nat. Commun.* **2011**, *2*, 509; b) H. M. M. ten Eikelder, A. J. Markvoort, T. F. A. de Greef, P. A. J. Hilbers, *J. Phys. Chem. B* **2012**, *116*, 5291 – 5301.

[20] J. Rezáč, P. Hobza, *J. Chem. Theory Comput.* **2012**, *8*, 141 – 151.

[21] a) MOPAC2012, J. P. Stewart, Computational Chemistry, Version 15.180 M, HTTP://OpenMOPAC.net; b) J. D. C. Maia, G. A. U. Carvalho Jr., C. P. Mangueira, S. R. Santana, L. A. F. Cabral, G. B. Rocha, *J. Chem. Theory Comput.* **2012**, *8*, 3072 – 3081.

[22] H. Kar, D. W. Gehrig, F. Laquai, S. Ghosh, *Nanoscale* **2015**, *7*, 6729 – 6736.

[23] T. C. Johnstone, S. J. Lippard, *J. Am. Chem. Soc.* **2014**, *136*, 2126 – 2134.

Received: January 14, 2016
Published online on April 26, 2016